NASA - Langley

SUMMARY OF STATIC AERODYNAMIC CHARACTERISTICS OF PARAWINGS

By William C. Sleeman, Jr., Delwsin R. Croom
and Rodger L. Naeseth

This presentation will summarize some of our recent work on the static aerodynamic characteristics of parawings. It appears advisable to acquaint you with some of the terminology used in this presentation and several that will follow, so we will go to the first slide.

SLIDE 1

This slide shows a typical parawing with a conical shaped canopy. The leading edges and keel may be rigid or flexible members and the wing may or may not have a spreader bar to hold the wing sweep angle fixed. In this talk, and others, reference is made to the flat planform sweep and the dotted lines in the lower figure show the flat sweep. In constructing these wings, the fabric for the canopy is cut to the desired flat pattern sweep. When the sweep is increased to the flight sweep, two lobes are formed which have approximately conical shape in flight. The aerodynamic coefficients are based on the area of the flat planform and the keel length.

In some cases, flutter of the fabric at the trailing edge has necessitated the use of a bolt rope in the hem at the trailing edge as shown here.

SLIDE 2

The next slide summarizes some of the most important beometric parameters that we have investigated on parawings.

(Read from chart)

We are not going to talk about all of these items but we have selected several to illustrate the type of work that we are doing and to indicate the present state-of-the-art as regards maximum lift-drag ratios.

SLIDE 3

Let us now look at some familiar aerodynamic parameters. The next slide presents the lift-curve slope and $C_{L_{max}}$ as a function of flight sweep for a 45° flat pattern sweep. These results were obtained in a systematic planform study in which wing sweep was the primary variable on wings having rigid members. The little sketches show that as the sweep increased, the height of the lobes of the canopy increase.

The experimental and theoretical lift slopes are seen to be in very good agreement. The maximum lift coefficient for 50° sweep was about 1.1 and it decreased with increasing sweep. $C_{L_{max}}$ was not determined for the higher sweeps because C_L was still increasing with up to $\alpha = 55^{\circ}$, which was the limit of the test setup.

SLIDE 4

We go now to maximum lift-drag ratios obtained in the same planform study and the next slide presents the variation of L/D_{max} with sweep angle. Experimental results are shown by this curve and the dotted curve indicates an estimated upper bound, using theory for a conventional flat wing and an assumed skin friction drag of .013. We see that there is a considerable gap between the experiment for conical canopies and the theory for flat wings; and we will spend some time discussing why these differences are shown and how we might be able to raise the level of the experimental data.

We have not indicated a theoretical estimate for conical shaped wings because the lift-drag ratios are greatly influenced by several design factors other than the wing planform sweep and aspect ratio. Of course, as for conventional wings, the wing sweep and aspect ratio are among the most important factors, but for flexible wings, the canopy shape can be of equal importance to these primary variables. Other important factors affecting $(L/D)_{max}$ are the way the fabric is attached at the leading edge, the leading edge size and shape. We will discuss these effects briefly, but first I would like to point out that we are discussing wing-alone characteristics and the lift-drag ratios will be reduced by the addition of a payload and its connecting members. The amount of this reduction in L/D will, of course, be a function of the wing loading or relative size of the payload and wing.

SLIDE 5

The next slide shows the importance of the details of the leading-edge geometry for a 55^{o} swept wing. Let's consider first, the effect of leading-edge diameter. This curve shows that reducing the diameter from 7-percent keel to 1.5-percent keel increased the L/D_{max} from 4.6 to 6.3. Next, let's look at the effect of how the fabric is attached to the leading edge. This is shown by the shaded symbols which show both the L/D_{max} and how the fabric was attached for a leading-edge diameter of 7-percent keel. Here we see that the L/D can be increased from about 3.5 to 4.6 by moving the fabric attachment from the bottom to the top of the leading edge.

These results indicate therefore that to get the best L/D_{max}, you want to minimize the leading-edge diameter and have the fabric attached at the top of the leading edge. Now, if you can't minimize the circular diameter for structural reasons, the, perhaps an airfoil shaped leading edge could be used. The plot on the right shown how L/D_{max} varies with airfoil thickness ratio on the leading edge. The value of t/c = 1.0 is the 3-percent circle shown on the left-hand plot. In these tests, the thickness remained constant (3-percent keel) and the chord was increased to obtain this variation of thickness ratio. These results show that the use of an airfoil section at the leading edge can provide gains in L/D_{max}.

SLIDE 6

Let's turn now to another facet of our systematic planform study in connection with lift-drag ratios. The next slide shows the effect of flat pattern sweep for a given flight sweep of 60°. We see that the lift-drag ratios show a consistent decrease as the canopy lobes become larger. One of the main reasons for this decrease in L/D is that as the wing surface becomes more and more conical, the wing has more twist across the span, and the twist may amount to as much as 40° or 50° washout. This very high twist can cause the tip sections to carry negative lift at low and moderate angles of attack, which would cause high induced drag. Here, we see that the wing having the highest L/D has the least twist and perhaps we could approach the ideal curve for L/D_{max} shown previously by making the wing flat. This would be fine, but we would be back to a conventional wing requiring a heavier structure. Some of our latest work has been

directed toward optimizing L/D on flexible wings by using wing canopies formed about a cylinder with its axis parallel to the keel.

SLIDE 7

This photograph shows one of these wings in the wind tunnel. The scmitar-shaped leading edge gives the same fabric height at the leading edge as at the trailing edge and the wing consequently has no twist or camber across the wing span. These members were used for expediency in the tests to hold the wing sweep fixed, in place of the more common spreader-bar installation. The forces on these members was substracted out of the data. Our next slide presents data for this wing, and others, and indicates the present state-of-the-art as regards L/D.

SLIDE 8

Here we have summarized measured lift-drag ratios for flexible parawings having both conical and cylindrical canopy shapes. This curve shows that an L/D of approximately 5 can be expected from an aspect-ratio 2.8 parawing having a conical canopy. The use of cylindrical canopy on this wing planform increases the maximum lift-drag ratio to a value of 10.

Now, a more obvious means for increasing L/D would be to increase the aspect ratio, and results are shown for an aspect-ratio-6 parawing with the two canopy shapes. Here we see that increasing the aspect ratio from 2.8 to 6 for the conical canopy produced an increase in $(L/D)_{max}$ from a value of 6 to a value of 8. And then, going from the conical to the cylindrical canopy with the aspect-ratio-6 wing gave a maximum value of lift-drag ratio of 14.

We would like to point out that no particular planform shown here should be considered the optimum parawing because for some applications, the L/D at high lift would be of greater importance than the maximum value of L/D. For example, the conical canopy provides higher L/D at high lift because the washout alleviates the tip stall. Our work on high performance parawings will be continuing in efforts to extend the L/D envelope in this direction (up and to the right).

In the selection of a wing configuration for a particular application, other factors such as structural weight trade-offs and complexity have to be evaluated in addition to the aerodynamic characteristics. Some of these structural loads considerations will be discussed by Mr. Taylor in one of the following talks.

SLIDE 9

Let's turn now from the subject of lift-drag ratios to other phases of our work on parawings. The next slide presents some typical lateral stability characteristics obtained in the wing planform studies. Inasmuch as the center of gravity for parawing applications is located a considerable distance below the wing, the moment reference for these stability parameters is positioned as shown.

These data are presented for the purpose of indicating the magnitude of these lateral derivatives throughout the sweep range. The importance of these derivatives will be discussed later in the presentation by Mr. Johnson.

SLIDE 10

Let's now consider a factor more akin to the sailmaker's art than wind-tunnel aerodynamics, but nevertheless of importance in the overall problem of obtaining a satisfactory canopy for a parawing. The next slide shows the effect of orientation of the fabric weave on the canopy shape.

These views were taken from a wind-tunnel study of identical wing planforms in which the only variable was fabric orientation. Straight-line grids were drawn on the flat pattern of each canopy and photographs were made at each test angle of attack. There was little difference in the aerodynamic characteristics but we see that the canopy in which the warp was parallel to the trailing edge had a smooth shape throughout most of the angle-of-attack range.

When the threads were run parallel to the keel, however, the canopy had an appreciable bulge in this area because the threads from the tip, rearward were not attached to a structural member. At low angles of attack this model had appreciable trailing-edge flutter and the first canopy was torn in shreads.

We have always made our canopies with the weave running parallel to the trailing edge and you may wonder why we have brought up the subject of fabric orientation. Well, most of the models we have received from contractors have had the fabric weave running parallel to the keel and we have encountered the same fabric distortion and trailing-edge flutter. Indications are that the fabric distortion can cause travelling waves in the canopy that start near the apex and move rearward. This could cause troublesome variations in control force at a given trim lift.

Our experience has been substantiated in work the Ryan people have done on the powered test vehicle. After installing their second canopy, which had the weave parallel to the keel, they had to install a boltrope and several batters in the rear part of the canopy to stabilize the fabric distortion.

SLIDE 11

Now, on some of our models, particularly those with flexible leading edges, we have found the use of a trailing-edge boltrope desirable. The next slide shows the effects of boltrope length on pitching moments and lift coefficients. For the 0-percent case, the boltrope length is equal to the length of the fabric trailing edge. The other curves are for the boltrope 2-percent and 4-percent shorter than the trailing-edge length.

Pitching-moments are presented about a moment reference on the wing keel 50-percent back from the apex, and we see that shortening the boltrope gives a fairly constant increment of C_m and C_L through most of the angle-of-attack range. These characteristics suggest that varying the boltrope length may be an effective means for longitudinal control.

SLIDE 12

Thus far, we have considered only the characteristics of the wing alone. The next slide shows some longitudinal characteristics in pitch of a complete configuration in which an inflated tube parawing is used in the recovery of the Gemini capsule. In these tests the capsule was mounted to a sting support through a six-component strain-gage balance. The wing was rigged for two different flight conditions, based on aerodynamic characteristics obtained from our general parawing research program. For these tests, the wing was in flight, and its attitude and position were determined by the aerodynamic forces on the wing and the restraint of the cable rigging.

The glide configuration was selected to trim the configuration near L/D_{max} with the capsule at an angle of attack of 18° and the wing at 20°. In the rigging for the landing configuration the front cable was lengthened and the wing rotated to an angle of attack of 45°. The capsule angle for the landing is 0° to enable the capsule to touch down on skids.

We see that the estimated rigging for these conditions produced approximately the desired trim angle of attack. The lift-drag ratios are low, mainly because of the large diameter inflated tube leading edges used. $(L/D)_{max}$ for the wing alone was about 3.4.

We would like to point out that these results are applicable only at the trim conditions because, in order to change the lift coefficient a different rigging would be required. We are not certain of the significance of these results, such as the break-in pitching moments below trim. If these moments are indicative of the flight vehicle, then we may have cause for concern; however, our flight tests of inflated tube models have not indicated difficulties in this area.

We believe that there are limitations in static wind-tunnel tests of this nature and more work is needed to establish proper testing techniques to provide static data that can be properly interpreted.

SLIDE 13

In the design of the Gemini recovery system, estimates had to be made of cable tension loads in order to size the cables properly. It would appear desirable to rig the wing so that the cable loads were more or less equally distributed. Now, these estimates involve assumptions and uncertainties and it was desirable to get an experimental check on these cable loads.

The next slide presents some cable tension loads in terms of the percent of total load for each cable. Data are shown for the landing configuration where the loads were the highest. We see that the loads in the cables going to the center keel were about the same at the design capsule angle of 0^{o} with the lines going to the leading edges carrying a somewhat higher percent of the load.

For angles below the design point the diagonal line tends to go slack and for angles above 0^{o}, the diagonal loads up rapidly and the front line tends to go slack.

These data are believed to be subject to the same limitations mentioned in connection with the previous slide with regard to tunnel test technique. We believe, however, that these results are useful in evaluation cable loads for the design point and furnish a valuable reference for assessing the estimated loads. I would also like to mention that when we resolved these loads into lift and drag components and computed the summation of pitching-moment contributions, we got excellent agreement with the results presented in the preceeding slide.

CONCLUDING REMARKS

I believe that we should bring this presentation to a close now with a brief recall of some of the salient points covered. First with regard to lift-drag ratios:

(a) In addition to the expected effects of wing aspect ratio and sweep on $(L/D)_{max}$, the canopy shape was found to have a first order effect on this parameter, also.

(b) The details of the fabric attachment and leading-edge size and shape have an important effect on $(L/D)_{max}$.

(c) Lift-drag ratios for a low-aspect-ratio parawing can approach closely those of a flat wing of the same aspect ratio if an untwisted cylindrical-canopy shape is used. $(L/D)_{max} = 10$ for aspect ratio 2.8.

(d) A value of $(L/D)_{max}$ of 14 was obtained with an aspect-ratio-6 parawing having a cylindrical canopy.

Next, the fabric orientation was shown to be important; for a smooth canopy contour, the weave should be parallel to the trailing edge.

And finally we discussed some model tests results of the Gemini configuration and pointed out some limitations of static wind-tunnel tests for this type of cable-supported configuration.

TYPICAL PARAWING

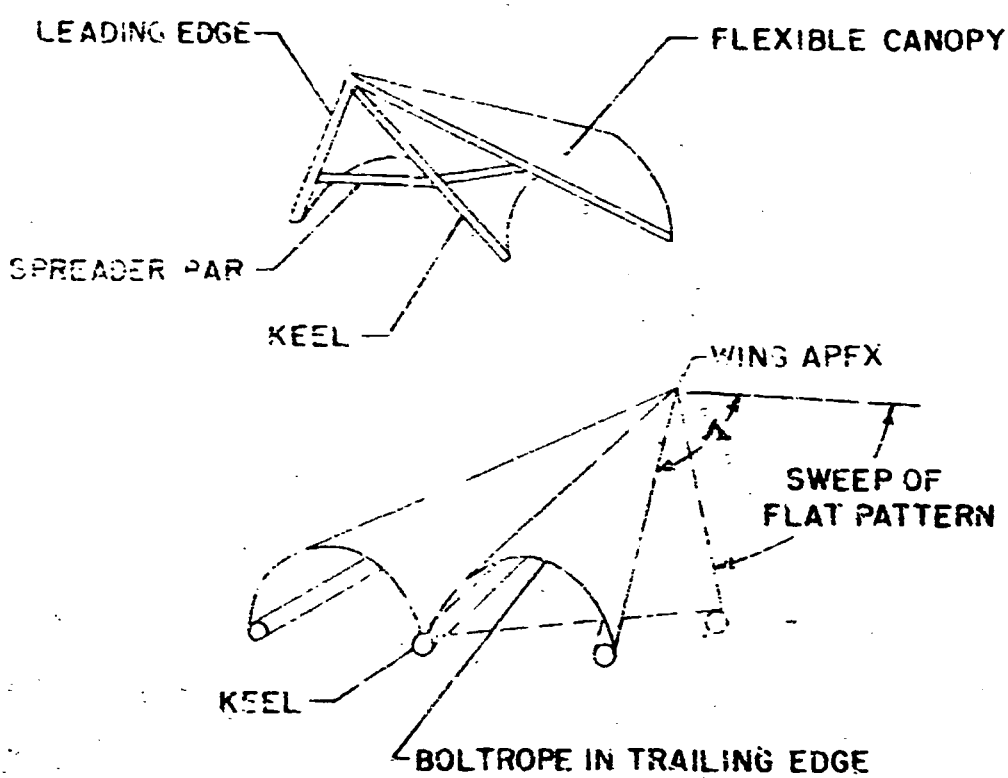

SUMMARY OF GEOMETRIC PARAMETERS STUDIED IN STATIC WIND TUNNEL TESTS OF PARAWINGS

A. WING PLANFORM
- SWEEP 41° TO 75°
- ASPECT RATIO 1.0 TO 6.0
- TAPER RATIO 0

B. WING LEADING EDGE
- SECTION: C AND ⊂⊃
- DIAMETER: 1.5% TO 7.0% l_k
- FABRIC ATTACHMENT

C. CANOPY SHAPE
- CONICAL TWIST & CAMBER
- CYLINDRICAL ZERO TWIST AND CAMBER

D. SPREADER BAR
- NO BAR
- SIZE & SHAPE
- LOCATION

E. CONTROLS
- WING SHIFT (C.G. MOVEMENT)
- WING TIP DEFLECTION
- BOOTROPE
- LEADING EDGE DEFLECTION

F. CANOPY FABRIC ORIENTATION

FABRIC WEAVE PARALLEL TO:
1. KEEL
2. TRAILING EDGE

G. COMPLETE CONFIGURATIONS
1. RYAN POWERED VEHICLE
2. MICROMETEOROID EXPERIMENT
3. SATURN BOOSTER
4. GEMINI RECOVERY
5. AUXILIARY WING FOR AIRCRAFT

AERODYNAMIC CHARACTERISTICS OBTAINED

C_L, C_D, C_m, L/D, C_{L_α}, $C_{L_{MAX.}}$, C_{l_β}, C_{n_β}, C_{Y_β}, PRESS. DIST., CABLE TENSION, CONTROL EFFECTIVENESS

EFFECT OF PARAWING LEADING EDGE SWEEP ON C_{L_α} AND $C_{L,max}$.

45° FLAT PLANFORM SWEEP

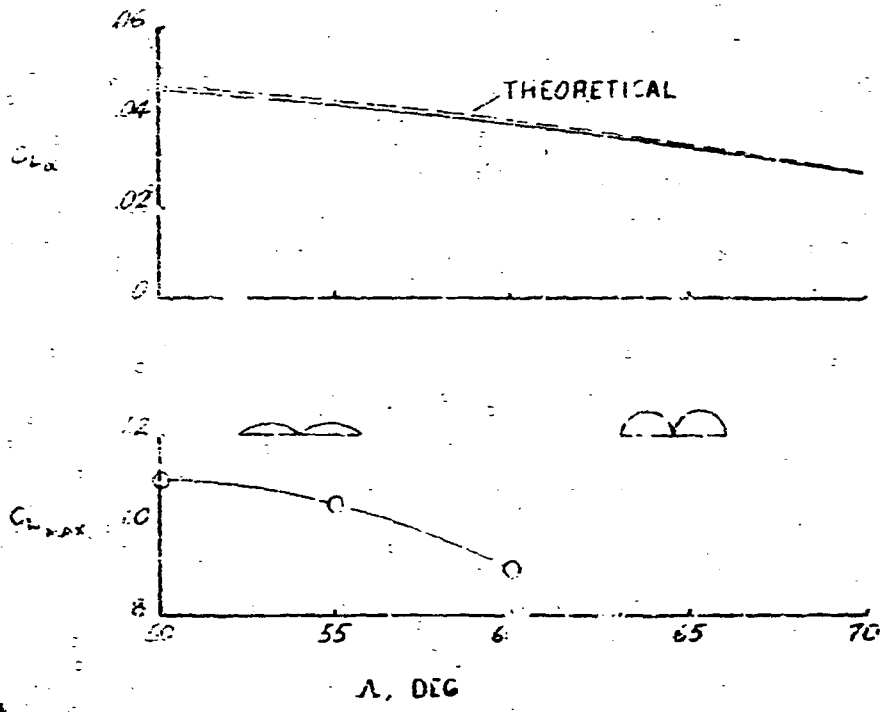

NASA LANGLEY

EFFECT OF PARAWING LEADING EDGE SWEEP ON $(L/D)_{MAX}$ 45° FLAT PLANFORM SWEEP

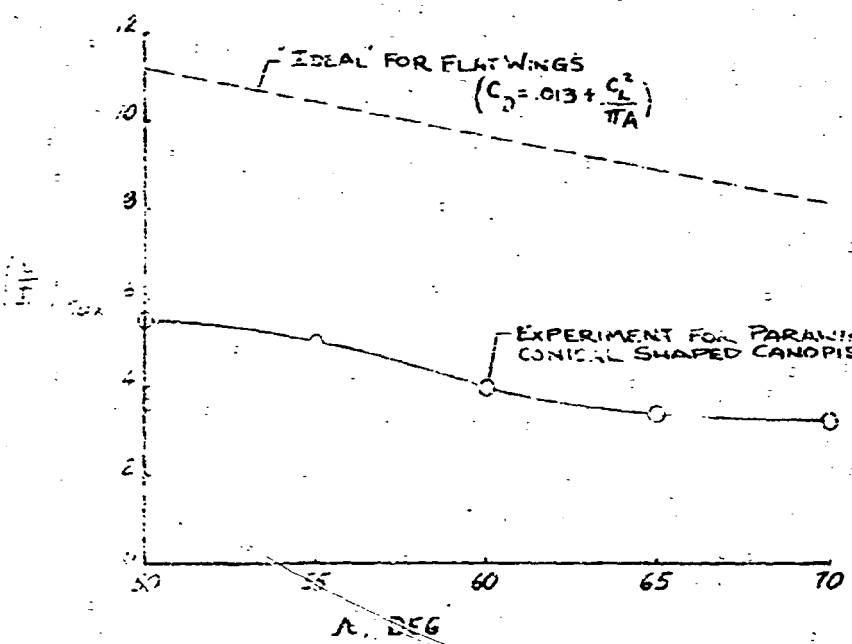

4

EFFECT OF LEADING EDGE DIA., FABRIC ATTACHMENT, AND L.E. THICKNESS RATIO ON $(L/D)_{MAX.}$

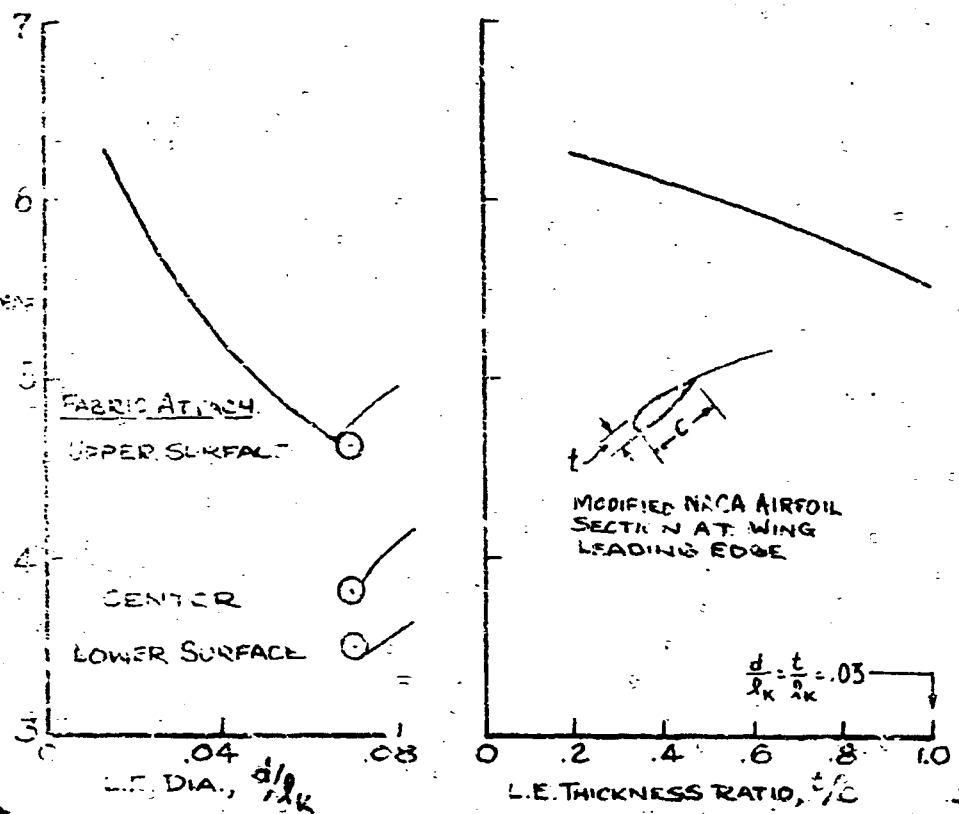

EFFECT OF CANOPY SIZE
IDENTICAL PROJECTED PLANFORM

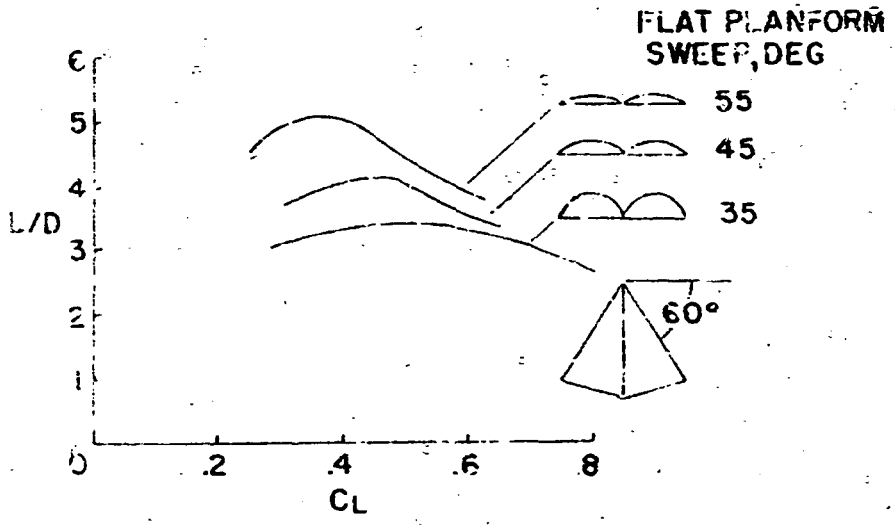

L/D VALUES FOR PARAWINGS WITH CONICAL AND CYLINDRICAL SURFACES

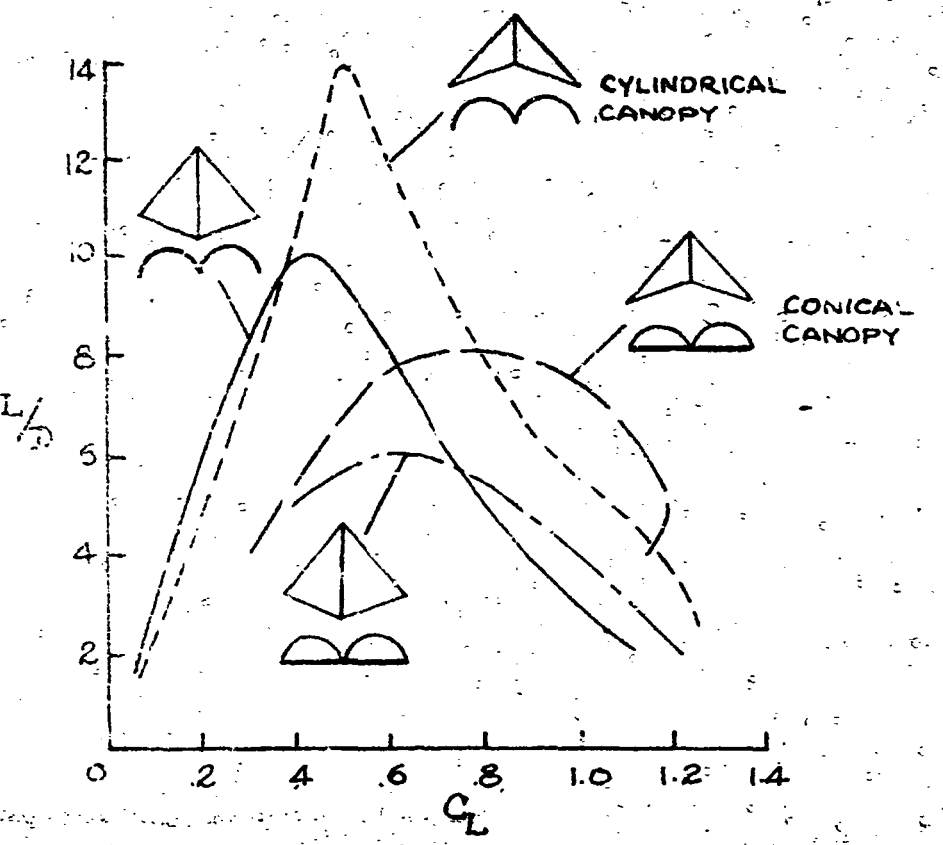

EFFECT OF SWEEP ON WING-ALONE LATERAL-STABILITY PARAMETERS

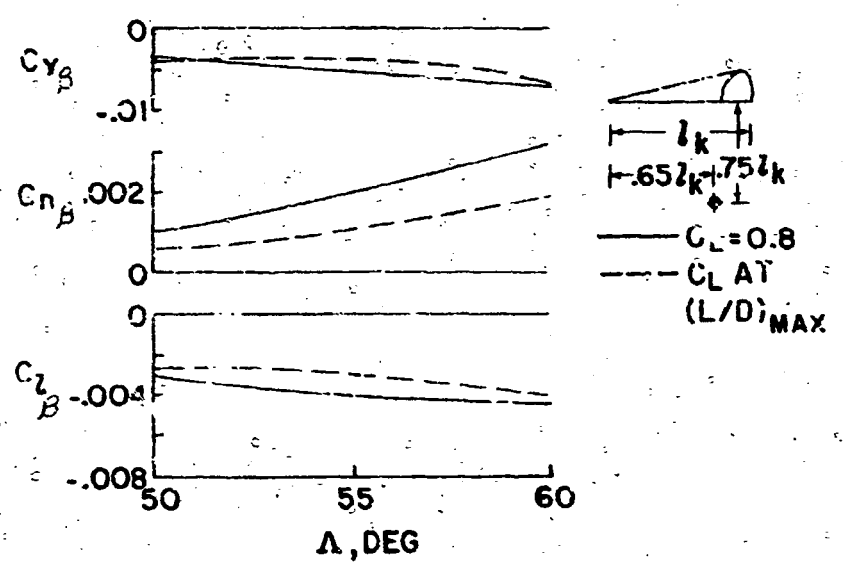

EFFECT OF FABRIC ORIENTATION ON CANOPY SHAPE

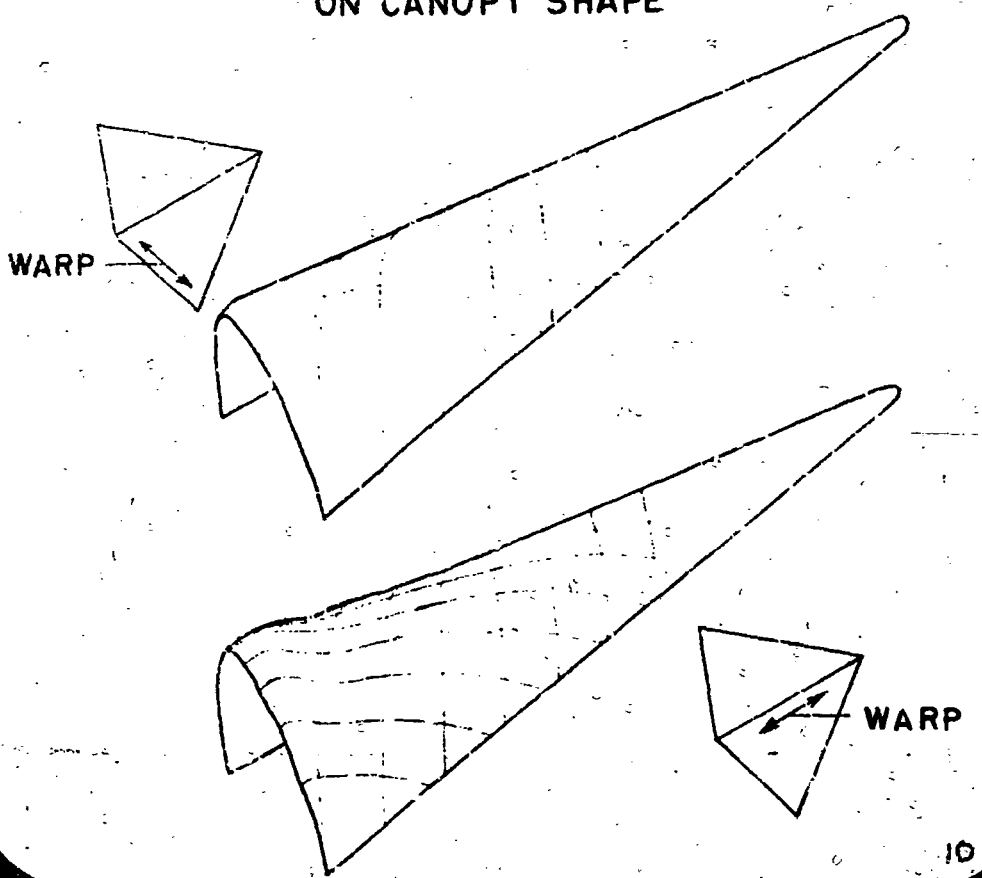

EFFECTS of BOLTROPE SHORTENING

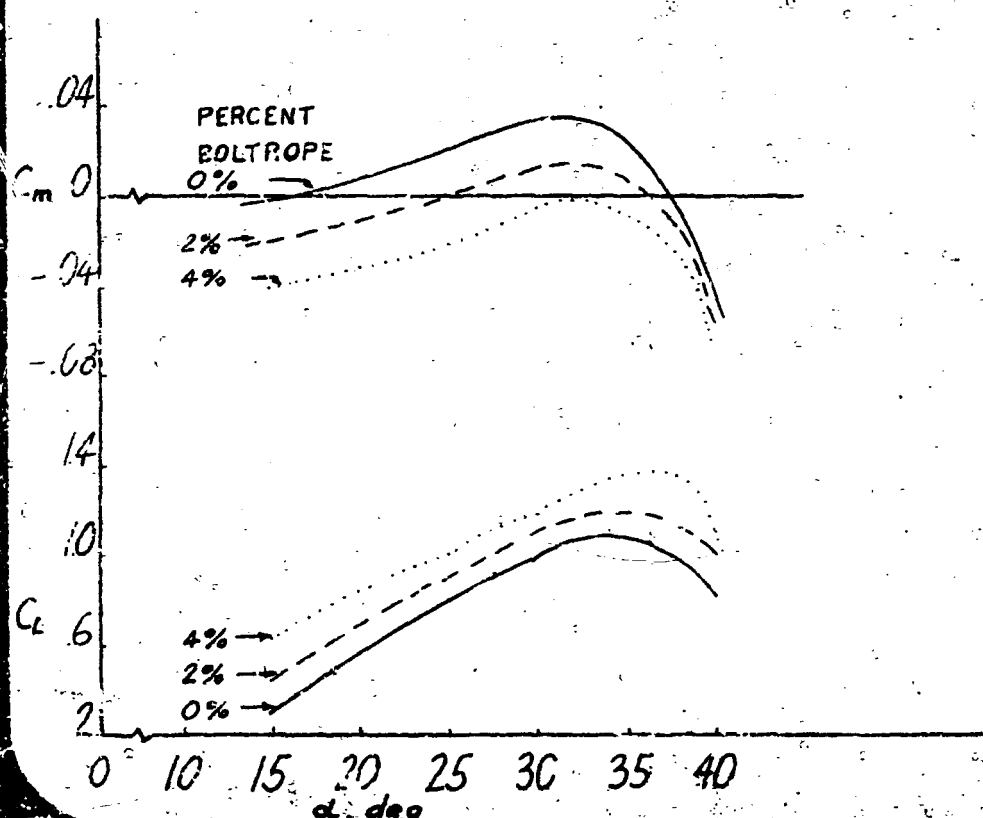

GEMINI-PARAGLIDER CHARACTERISTICS

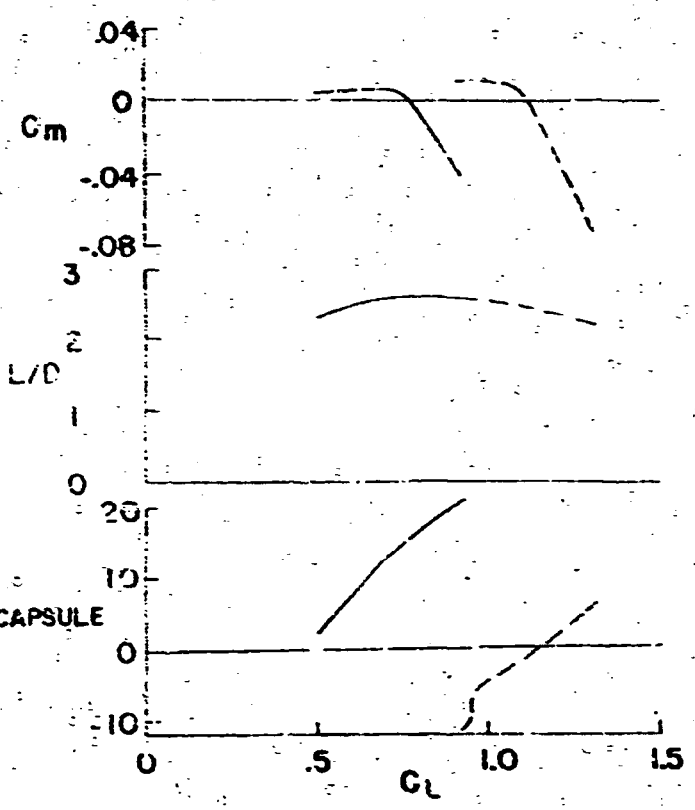

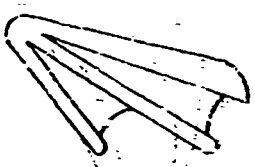

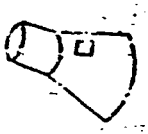

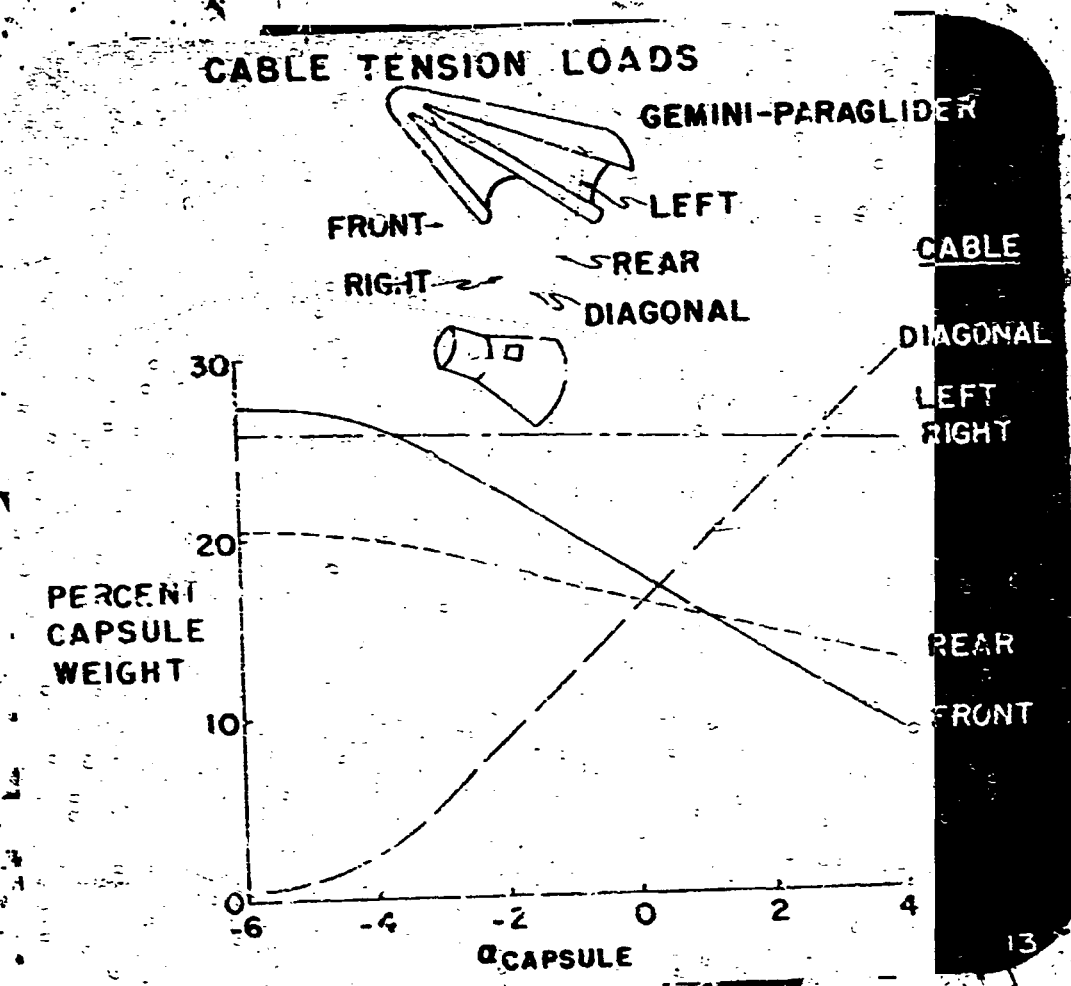

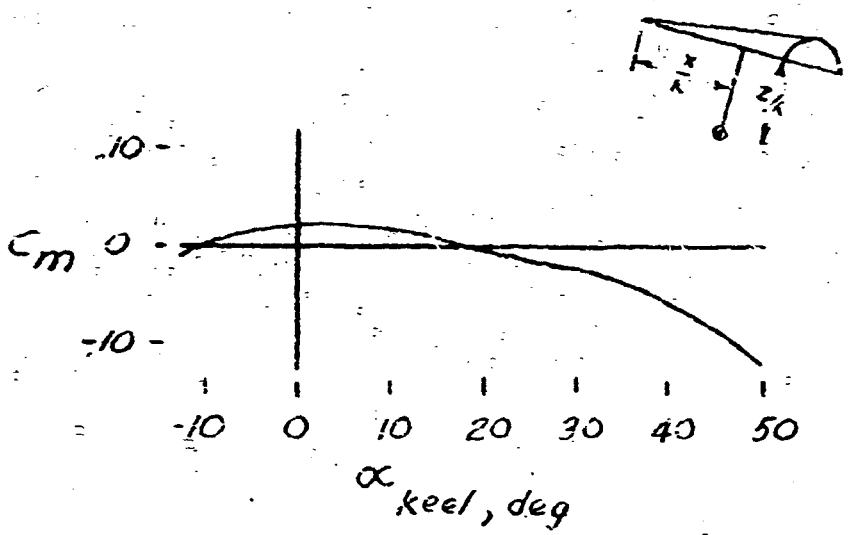

Fig. 1

NASA-LANGLEY

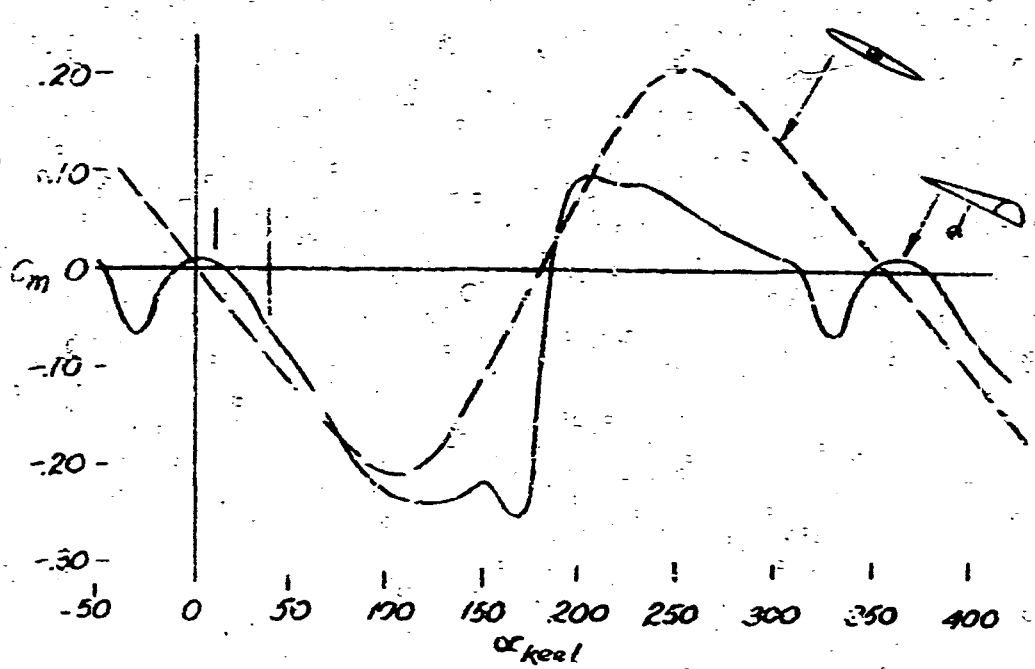

Pitching moment characteristics

Fig. 2

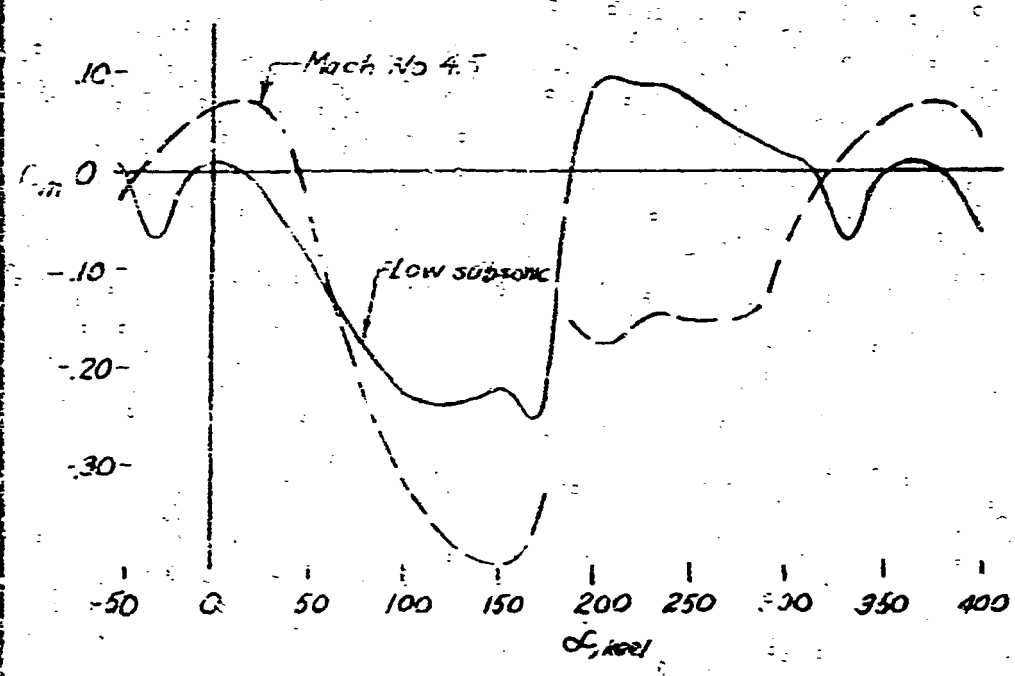

Pitching moment characteristics

Fig. 3

NASA-LANGLEY

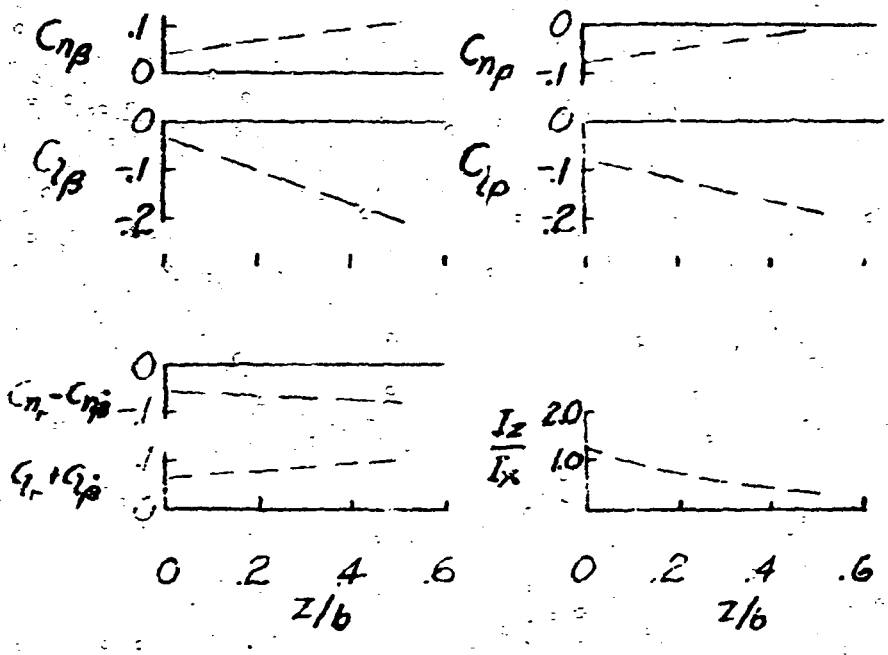

LATERAL STABILITY PARAMETERS

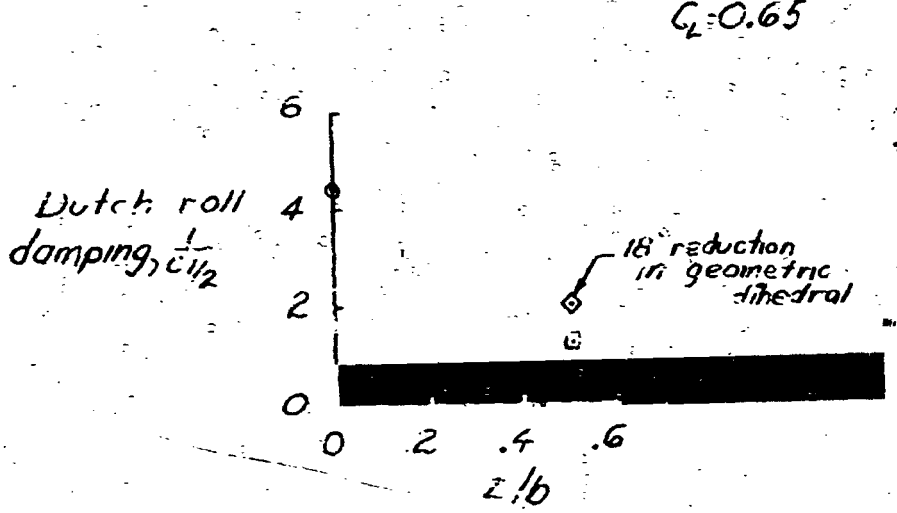

CALCULATED DUTCH ROLL DAMPING

Fig. 5

NASA-LANGLEY

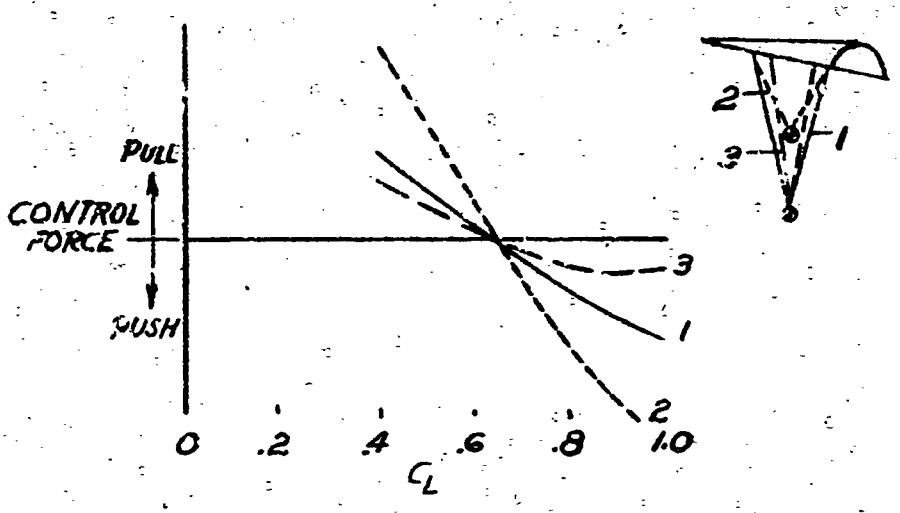

Longitudinal control force characteristics

Fig. 6

NASA-LANGLEY

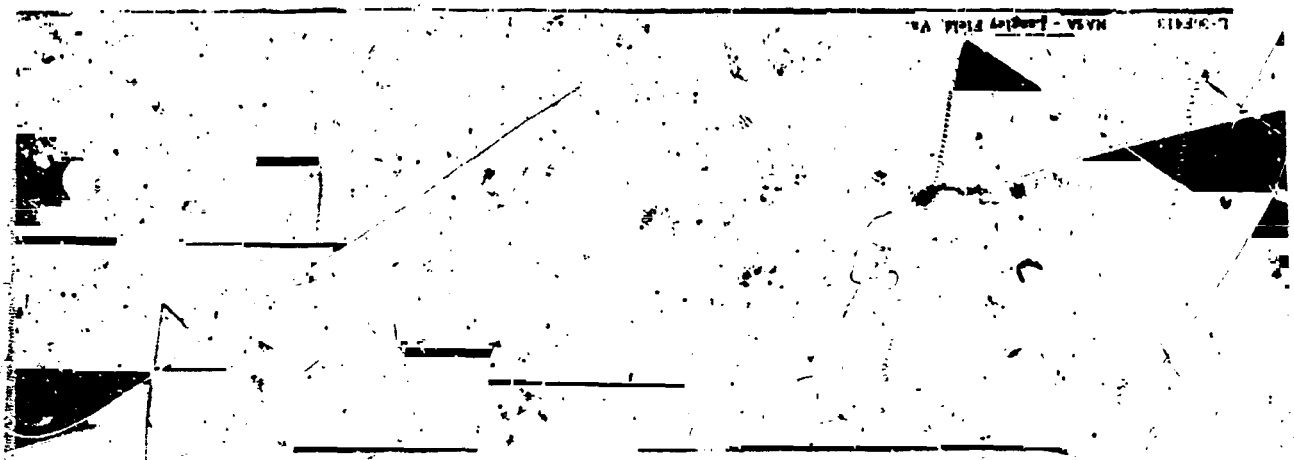

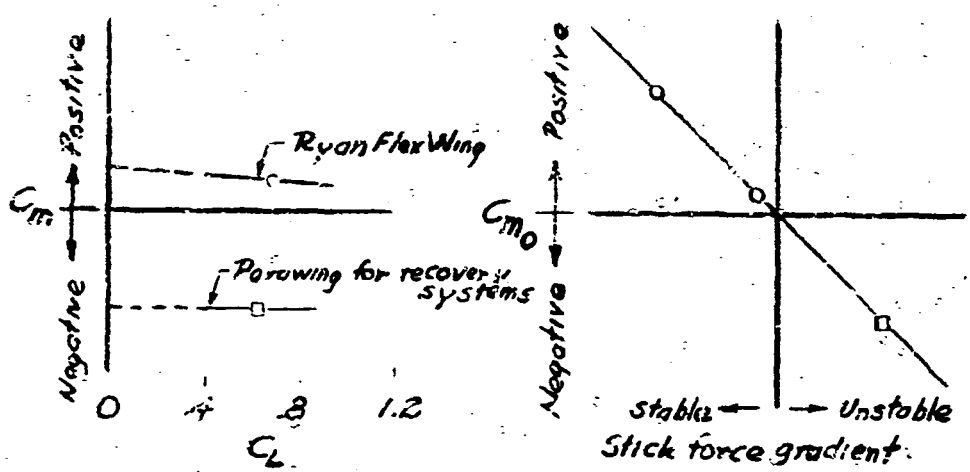

Effect of C_{m_0} on longitudinal stick force gradient

Fig. 7

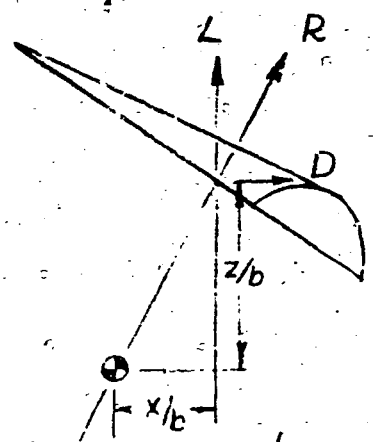

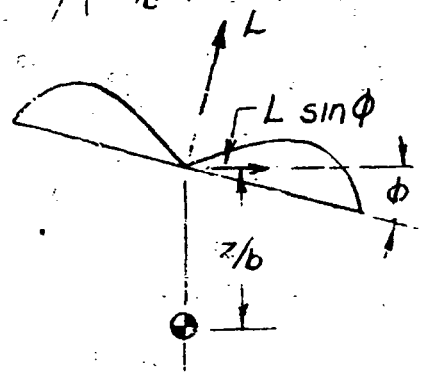

$C_l = C_L \sin\phi \, z/b$

$C_n = C_L \sin\phi \, x/b$

$$C_{l_{net}} = C_L \sin\phi \, z/b \left(1 - \frac{-C_{l_\beta}}{C_{n_\beta} \frac{z}{b}}\right)$$

LATERAL CONTROL EQUATION

Fig. 8

NASA-LANGLEY

L.E. thickness, percent keel
——— 1.5
- - - - 7.5

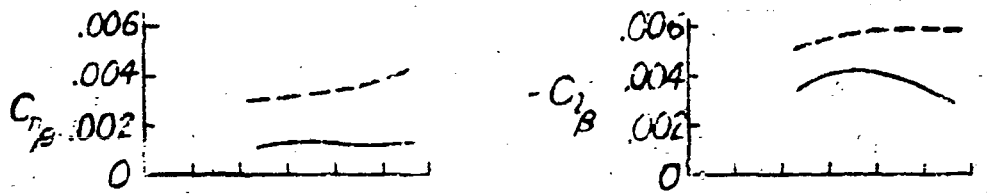

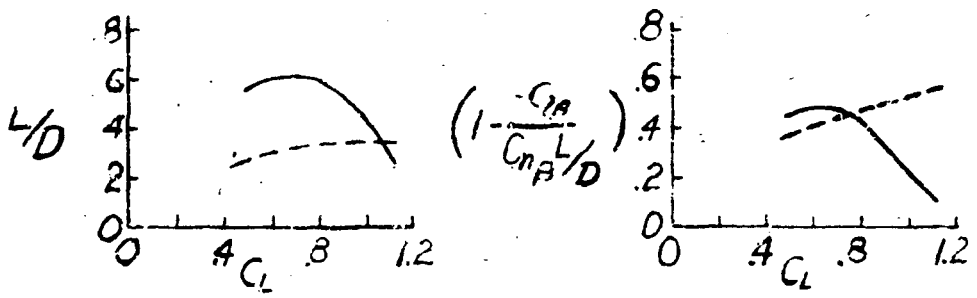

LATERAL CONTROL FACTORS

Fig. 9

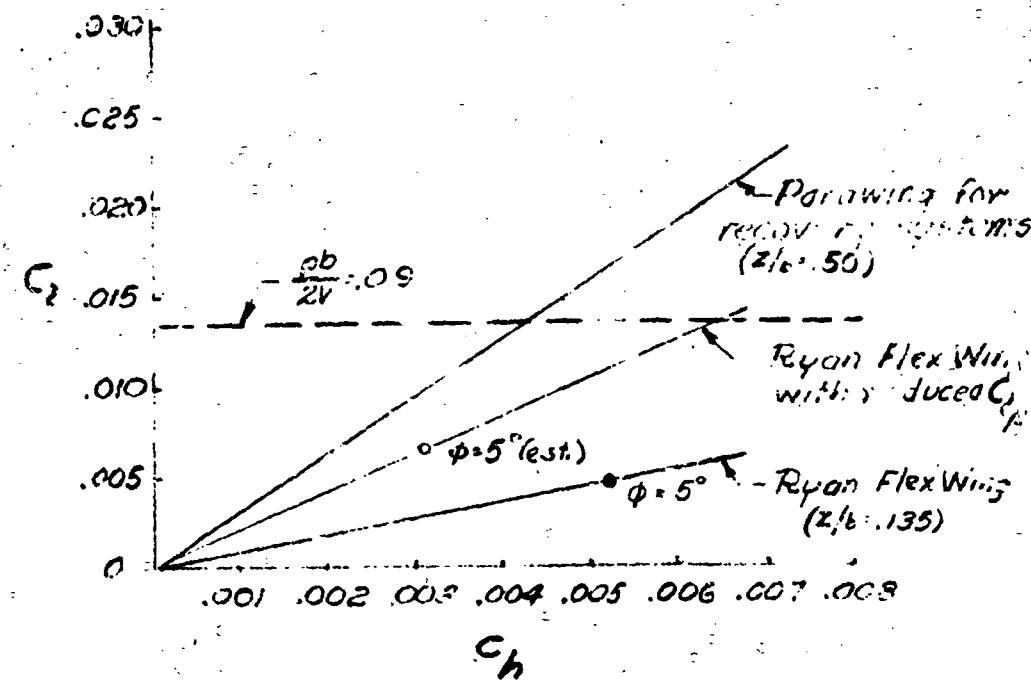

ROLLING MOMENT AND HINGE MOMENT
RELATIONSHIP

Fig. 10

ALTERNATIVE CONTROL METHODS

1. Trailing edge bolt rope
2. Trailing edge risers
3. Hinged leading-edge and keel members
4. Auxiliary surfaces

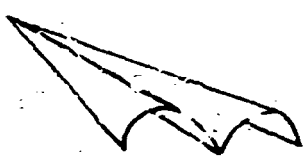

NASA-LANGLEY

Fig. 11

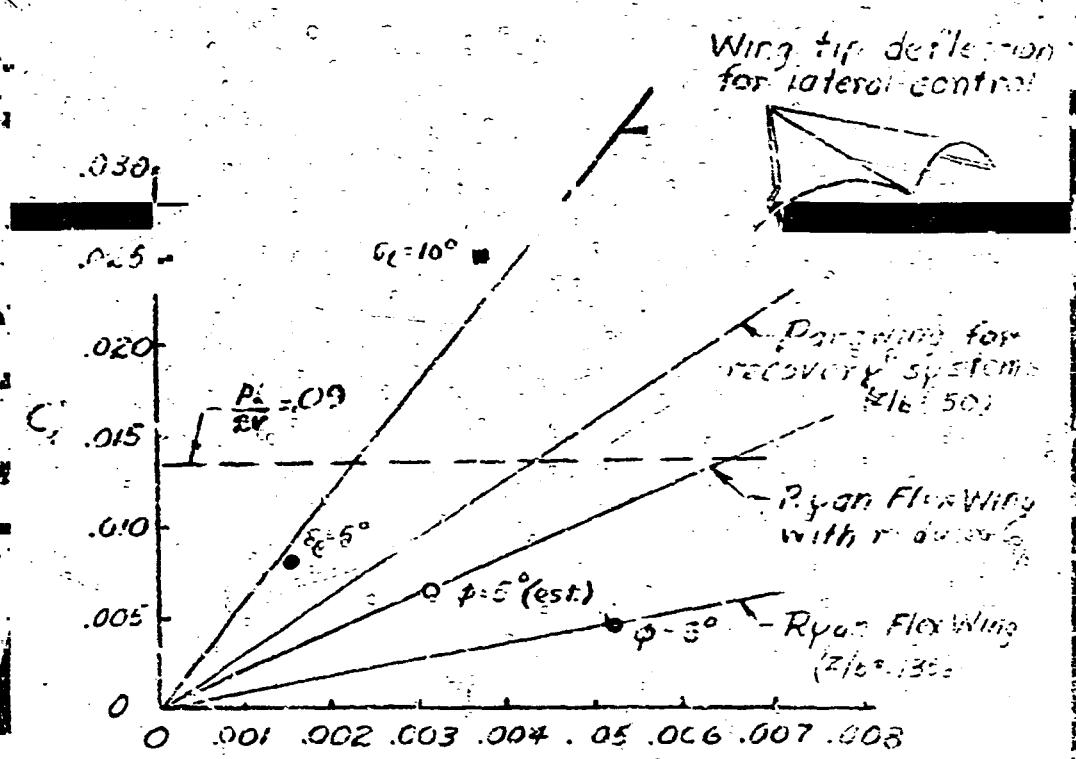

ROLLING MOMENT AND HINGE MOMENT RELATIONSHIP

NASA - Langley Field, Va.

Fig 12

NASA-LANGLEY